

Discovery of another peculiar radial distribution of Blue Stragglers in Globular Clusters: The case of 47 Tuc¹

Francesco R. Ferraro², Giacomo Beccari², Robert T. Rood³, Michele Bellazzini⁴, Alison Sills⁵, Elena Sabbi²

ABSTRACT

We have used high resolution *WFPC2-HST* and wide field ground-based observations to construct a catalog of blue straggler stars (BSS) in the globular cluster 47 Tuc spanning the entire radial extent of the cluster.

The BSS distribution is highly peaked in the cluster center, rapidly decreases at intermediate radii, and finally rises again at larger radii. The observed distribution closely resembles that discovered in M3 by Ferraro et al (1993,1997). To date, complete BSS surveys covering the full radial extent (*HST* in the center and wide field CCD ground based observations of the exterior) have been performed for only these two clusters. Both show a bimodal radial distribution, despite their different dynamical properties. BSS surveys covering the full spatial extent of more globular clusters are clearly required to determine how common bimodality is and what its consequence is for theories of BSS formation and cluster dynamics.

Subject headings: Globular clusters: individual (47 Tuc); stars: evolution – blue stragglers – binaries: close;

¹Based on observations with the NASA/ESA HST, obtained at the Space Telescope Science Institute, which is operated by AURA, Inc., under NASA contract NAS5-26555. Also based on WFI observations collected at the European Southern Observatory, La Silla, Chile, within the observing programs 62.L-0354 and 64.L-0439.

²Dipartimento di Astronomia Università di Bologna, via Ranzani 1, I-40127 Bologna, Italy, ferraro@bo.astro.it

³Astronomy Dept., University of Virginia, Charlottesville, VA 22903-0818, USA; rtr@virginia.edu

⁴INAF - Osservatorio Astronomico di Bologna, via Ranzani 1, I-40127 Bologna, Italy, bellazzini@bo.astro.it

⁵Department of Physics and Astronomy, McMaster University, 1280 Main Street West, Hamilton, ON, L8S 4M1, Canada; asills@mcmaster.ca

1. Introduction

Blue straggler stars (BSS) are found primarily in star clusters, where they appear as a sparsely populated extension of the main sequence above the turnoff point. Superficially they appear to be main sequence stars with masses larger than expected for the cluster at its turnoff age. There are two proposed mechanisms thought to produce BSS: the first is mass exchange in a binary system and the second is the merger of two stars induced by stellar interactions (either single or in binaries) in a dense stellar environment. Globular cluster cores are obvious targets for BSS not only because of their high stellar density, but because primordial binaries in the clusters may well have sunk to the cores.

With the advent of the Hubble Space Telescope (*HST*) it became possible for the first time to search dense cluster cores for BSS. Searches in the ultraviolet (UV) can be particularly effective, not because BSS are especially bright in the UV, but because the red giants are faint in the UV. The photometric blends which mimic BSS in visible CMDs are far less problematic in the best UV CMD planes, and it is possible to obtain complete BSS samples in even the densest cores. With *HST*, the densest cluster cores are *the obvious place* to search for BSS, and there have been few systematic searches for BSS in the outer parts of clusters in recent years. Indeed only one cluster, M3, has been adequately surveyed for BSS over its entire radial extent (Ferraro et al. 1993; Ferraro et al. 1997).

Since it is a massive cluster with high central density, 47 Tuc is an obvious target for a BSS search, and its core has been the subject of several earlier investigations (Guhathakurta et al. 1992; de Marchi et al. 1993; Ferraro et al. 2001; Knigge et al. 2002). These studies have covered only a fraction of the core either because they used the Faint Object Camera or just the PC of WFPC2. Albrow et al. (2001) found BSS in their WFPC2 search for eclipsing binaries in the core of 47 Tuc. Blue stragglers have also been studied outside the core of 47 Tucanae by Sills et al. (2000) who also modeled the BSS formation rate. Kaluzny et al. (1998) note several BSS candidates in their CMD of 47 Tuc, and there are clear BSS candidates in the Strömrgren photometry of Grundahl et al. (2002). Only a small part of the cluster exterior was covered by these studies.

With new wide field imagers on ground based telescopes at sites with excellent seeing it is now possible to perform BSS surveys which yield complete samples over the entire extent of the cluster. Here we present results covering both the full cluster core using *HST* WFPC2, and the exterior of the cluster using the wide field imager at the ESO 2.2 m telescope.

2. Observations and data analysis

2.1. The data-set

The photometric data used here consist of two sets:

(i)—*High resolution set*—a series of public HST/WFPC2 images taken through the UV filter F218W and F439W (B). The images have been retrieved from the *ESO/ST-ECF Science Archive*, the automatic *Archive Association Procedure* which allows retrieval of a set of images taken in the same filter and in similar conditions. The images are automatically combined and cleaned of cosmic rays. The first part of this data-set (specifically the PC) has been already published in Ferraro et al (2001). Here we present the analysis of the entire data-set (PC, WF2, WF3, WF4). The information about the observing epochs, the proposal ID number, the filter, and the number of exposures can be found in Table 1 of Ferraro et al 2001. The photometric reductions of the high resolution images were carried out using ROMAFOT (Buonanno et al. 1983), a package developed to perform accurate photometry in crowded fields and specifically optimized to handle under-sampled point spread function (PSF) (Buonanno & Iannicola 1989) as in the case of the HST-WF chips.

PSF-fitting instrumental magnitudes have been obtained using the standard procedure described in Ferraro et al. (1997a, 2001). The final catalog of the F218W and F439W magnitudes was calibrated by using the zero-points listed by Holtzman et al. (1995).

(ii)—*Wide Field set*— a complementary set of multi-filter (B , V , I) wide field images was secured during an observing run at the 2.2m ESO-MPI telescope at ESO (La Silla) in July 1999, using the Wide Field Imager (WFI). An additional data-set of public WFI images were also retrieved from the ESO/ST-ECF Archive. The WFI has exceptional imaging capabilities—each image consists of a mosaic of 8 CCD chips (each with a field of view of $8' \times 16'$) giving a global field of view of $33' \times 34'$.

The raw WFI images were corrected for bias and flat field, and the over-scan region was trimmed using standard IRAF⁶ tools. The PSF fitting procedure was performed independently on each V , B and I image, using DoPhot (Schechter et al. 1993). For each passband at least 7 exposures were combined, and the resulting magnitudes transformed to the same (instrumental) photometric system; stars in common were then averaged with the requirement that only stars successfully measured at least in 3 images per filter were included in

⁶IRAF is distributed by the National Optical Astronomy Observatory, which is operated by the Association of Universities for Research in Astronomy, Inc., under cooperative agreement with the National Science Foundation.

the final catalog. A final catalog listing the instrumental B , V , I magnitudes for all the stars in each field was finally obtained.

2.2. Astrometry

The entire catalog HST+WFI has been placed on the absolute astrometric system by adopting the procedure already described in other papers (see Ferraro et al 2001, 2003). The new astrometric *Guide Star Catalog (GSCII)* recently released and now available from the web (<http://www-gsss.stsci.edu/gsc/gsc2/GSC2home.htm>), was used to search for astrometric standard stars lying in the WFI image field of view. Several hundred *GSCII* reference stars have been found in the WFI FoV, allowing an accurate absolute positioning of the image. In order to derive an astrometric solution for each of the 8 WFI chips, we used a program specifically developed at the Bologna Observatory (P. Montegriffo et al 2003, in preparation). Then, a few hundred stars in the overlapping area between the WFI and the WFPC2 field of view were used as secondary astrometric standards in order to place the HST catalog in the absolute astrometric system. At the end of the entire procedure the rms residuals were of the order of $\sim 0''.3$ both in RA and Dec and we take this value as representative of the astrometric accuracy.

We used our standard technique (Montegriffo et al 1995, Ferraro et al 1999, 2001, 2003) to find the center of gravity (C_{grav}). The barycenter of resolved stars is compatible (within 1–2 arcsec) with the center of luminosity C_{lum} listed by Djorgovski & Meylan (1993). Thus in the following we use their value as center: $\alpha_{J2000} = 00^{\text{h}} 24^{\text{m}} 05^{\text{s}}.20$, $\delta_{J2000} = -72^{\circ} 04' 51''$.

3. Definition of the samples

In order to avoid spurious effects due to incompleteness of the ground based observations in the crowded central region of the cluster we restricted the WFI sample to the outer region $r > 130''$ (hereafter the *WFI sample*). In the inner $r < 130''$ our sample includes only stars in the WFPC2 FoV (hereafter the *HST sample*). This sample takes advantage of the superior capability of UV observations in detecting BSS (Ferraro et al 1999, 2001) in the overcrowded central regions of high density clusters. The Color-Magnitude Diagrams (CMDs) derived from these samples are shown in Figure 1 and Figure 2.

3.1. The BSS selection

Since the two data-set have been observed in different photometric bands, different selection boxes have to be defined to isolate the populations in the two CMDs. The definition of the BSS sample is quite natural in the UV-CMD (Figure 1) since, as usually seen, in these planes the BSS define a quite distinct sequence spanning ~ 3 magnitudes. A total of ~ 100 BSS have been identified in the HST-WFPC2 FoV. However, as in our previous studies of M3 and M80 (respectively, Ferraro et al 1997, hereafter, F97, and Ferraro et al 1999, hereafter, F99) to avoid any possible contamination due to blends, incompleteness etc, in the following we limit our analysis to the brightest portion of the BSS sequence. The faint threshold of the BSS selection box has been chosen to be $m_{218} < 18.7$. This limit is nearly 1 magnitude brighter than the cluster Main Sequence (MS) Turn-Off (TO) in the UV plane to avoid any spurious effect due to blends. The adopted selection box for the BSS in the HST sample is shown in Figure 1. 59 Bright-BSS (b-BSS) have been counted in this selection box.

In order to make a meaningful BSS selection in the WFI sample we converted the magnitude extension of the box defined in the UV plane into the ground-based $(B, B - V)$ and $(B, B - I)$ planes. The corresponding values have been computed by using the B filter which is in common in the two data sets (since the F439W WFPC2-filter is approximately a B filter). In doing this we first aligned the two CMDs in the $(m_{F439W}, m_{F218W} - m_{F439W})$ and $(B, B - V)$ planes, by using the the SGB and the HB level as reference, and then we determined the distribution of the selected bright BSS in B magnitude. This procedure gives a value of $B \sim 17.3$ and $B \sim 15$ for the faint and the bright threshold (respectively) of the BSS box in the WFI sample.

The color limits of the BSS box in the ground-based planes have been chosen to minimize the possibility of field contamination. The red edge has been assumed at $B - V = 0.5$, where a significative decrease of the galaxy field contribution is expected (see for example Figure 2 by Unavane et al (1996) and Figure 4 in Lemon et al., 2003). The blue edge has been chosen in order to exclude a few blue objects which lie significantly outside the BSS sequence (see Figure 2 (a)). This selection includes the bulk of the BSS population, while a few evolved BSS might be lost in the region dominated by the field population. However, as discussed in previous papers, the number of lost BSS is certainly small (see as example the case of M3 (Ferraro et al 1993, 1997)). We emphasize that even slightly different assumptions in the definition of the selection boxes would not alter the main results presented in this paper. With these limits an appropriate selection box for the bright BSS has been defined in the both the optical planes (see Figure 2- panel (a) and (b)). A preliminary selection of possible BSS has been done in the $(B, B - V)$ plane, but the the final selection has been done by using both $(B, B - V)$ and $(B, B - I)$ CMDs. Thus only the 57 objects which lie in the

BSS selection boxes in both the CMDs have been selected.

Figure 3 shows the final comparison of the BSS samples in the two data-set (HST and WFI, respectively) considered below. In order to make the two samples completely homogeneous, the faintest 6 BSS in the HST sample which fall just below the adopted threshold ($B \sim 17.3$) have been excluded. The final sample consists of 53 BSS in the HST sample and 57 BSS in the WFI sample (for a total of 110 objects).

3.2. The reference population

In order to study the behavior of the BSS with respect to the normal stars in the cluster, we have to select a reference population which is assumed to trace the cluster stars. As discussed in previous papers (see for example Ferraro et al 2003) the most *natural* reference population in the UV-CMDs is the Horizontal Branch (HB), since it is well separated from the other branches and HB stars are quite bright in most CMD planes (see Figure 1).

The selection of the HB is quite easy in both planes since it defines a well defined visible clump of stars in both the UV (see Figure 1 and also Figure 2 in Ferraro et al 2001) and the ground-based CMDs (Figure 2). Again the HB selection is defined independently in all the CMDs and is designed to include the bulk of the HB population. The HB box shown in Figure 1 and the selection shown in Figure 2 assure the inclusion of the bulk of the HB stars: small differences in the assumptions on the shape of the box would include or exclude a few stars. For example, a fainter level for the HB box in the UV plane would include a few scattered stars which might be RGB stars. In the ground-based planes (Figure 2) we designed an appropriate box to avoid the inclusion a small sequence of underluminous HB stars which are clearly lie below the ZAHB in Figure 2(a). Again the inclusion of these stars (which are less than a few percent of the global HB population) does not affect our conclusions in any way.

Following the criteria described above a total sample of 314 and 581 HB stars have been counted in the HB selection boxes, in the HST and WFI sample, respectively.

The global sample of 116 bright BSS and 895 HB stars spans almost the entire radial extension of the cluster (0 up to 23' from the cluster center) and is the largest sample ever published in 47 Tuc.

3.3. Field Contamination

Galaxy foreground contamination in the BSS region is negligible thanks to the selection in color ($B - V < 0.5$) see Figure 4 in Lemon et al (2003) and figure 2 by Unavane et al (1996). By using the star counts by Ratnatunga & Bahcall (1985) we estimate that ~ 100 field stars with $B - V < 0.8$ and $13 < V < 17$ are expected in the WFI FoV. Figure 2 by Unavane et al (1996) and Figure 4 by Lemon et al (2003) showed that the bulk of the Galaxy foreground stars are expected to have $B - V > 0.5$.

The brighter portion of the RGB of the Small Magellanic Cloud (SMC) field population is clearly visible in our CMD at $B = 18.2$, $B - V = 1.6$. Moreover the main contribution of the SMC background stars is expected at magnitudes significantly fainter than the BSS selection box (see Figure 1 by Zoccali et al. 2001). In any case the BSS selection box is located in the region between the Main Sequence (MS) of young stars and the evolved RGB stars (compare the BSS selection box and Figure 10 by Momany et al, 2001) where only a few SMC field stars are expected. In accord with the above considerations no correction has been applied to the BSS counts.

4. Results

As a first step the radial distribution of the 110 b-BSS has been compared to that of the reference population. The cumulative radial distribution for the 110 b-BSS and the 895 HB stars are plotted in Figure 4 (panel (a)) as a function of the projected distance from the cluster center. As can be seen the behavior of the two distributions is not monotonic since the BSS appear to be more concentrated than the HB in the central region and less concentrated than the HB in the outer region. Note that the shoulder visible in the radial distribution shown in Figure 4 (panel (a)) is due to the HST/Ground-based sample transition. As discussed above we conservatively decided to consider in the region $r < 130''$ only stars observed with HST. Because of the shape of the WFPC2 FoV there is a region at $r \sim 110 - 130$ where only a few stars can be detected. This region is indicated by a vertical shaded region in Figure 4 (panel (a)). The assumption of using only the HST sample in the most inner region of the cluster is, in our opinion, the safest possible choice, since the ground based magnitudes could be still severely affected by the crowding conditions at this distance from the cluster center. Note that this shoulder effect vanishes when the BSS population is scaled to a reference population (HB or RGB) or fractional luminosity as we do below.

The effect is better illustrated in Figure 4 (panel (b)) in which the radial distribution for two sub-samples HST and WFI are shown separately. As can be seen the BSS are

clearly more concentrated in the central region (HST sample) and less concentrated in the outer region (WFI sample) with respect to the reference HB population. A Kolmogorov-Smirnov test has been applied to the distributions to check the statistical significance of the difference. The test yields a probability of 99.96% (more than 3σ level of confidence) and 98.86% ($\sim 2.5\sigma$ level of confidence) that the b-BSS population has a different radial distribution with respect to the HB stars. This distribution closely resembles that already observed in M3 (F93, F97): indeed Figure 4 (panel (b)) is an almost exact copy of Figure 7 in F97. We accordingly follow the procedure described in F93 (applied also in F97) where the surveyed area has been divided into a set of concentric annuli. Thus, 11 concentric annuli (each containing roughly $\sim 10\%$ of the reference population) have been defined (see Table 1). The number of BSS and HB stars have been then counted in each annulus. The first observable quantity that can be measured in each annulus is the ratio $N_{\text{BSS}}/N_{\text{HB}}$.

Figure 5 (panel (a)) shows the distribution of this ratio as a function of the effective radius of each annulus. The distribution is clearly bimodal with the highest value in the innermost annulus. From this quite large value ($N_{\text{BSS}}/N_{\text{HB}} \sim 0.4$) the ratio significantly decreases to less than 0.1 as r increases and then slowly rises up in the outer region up to ~ 0.3 . Again this trend closely resembles that discovered in M3 by F97. In order to better analyze this trend we have computed the *relative frequency* of BSS and HB normalized to the fraction of luminosity sampled in each annulus. The fraction of light sampled in each annulus has been computed from the cluster brightness profile, and appropriately scaled to the the fraction of area covered by the observations in each annulus.

The original definitions by F93 are

$$R_{\text{BSS}} = \frac{(N_{\text{BSS}}/N_{\text{BSS}}^{\text{tot}})}{(L^{\text{sample}}/L^{\text{tot}})}$$

$$R_{\text{HB}} = \frac{(N_{\text{HB}}/N_{\text{HB}}^{\text{tot}})}{(L^{\text{sample}}/L^{\text{tot}})}$$

The numbers of BSS and HB in each annulus, the $N_{\text{BSS}}/N_{\text{HB}}$ ratio, the sampled luminosity and the specific frequencies defined above are listed in Table 1. The *relative frequency* of BSS as a function of the distance from the cluster center is then plotted in Figure 5 (panel (b)) and compared with the corresponding one for the HB “reference” stars. As can be seen, the HB specific frequency remain essentially constant over the surveyed area since the fraction of HB stars (as any post-main sequence stage) in each annulus strictly depends on the fraction of luminosity sampled in that annulus (see the relation by Renzini& Buzzoni 1986,

eq 2 in Ferraro et al 2003). In contrast, the BSS specific frequency reaches its maximum at the center of the cluster then decreases to an approximately constant value in the range $100''$ – $500''$ from the cluster center and then rises again. This behavior fully confirms the trend shown in Figure 5 (panel (a)) and suggests that dynamical events and/or formation mechanism shape the radial distribution of the BSS in the cluster (M. Mapelli et al. 2003, in preparation)

To further demonstrate the similarity with M3 and to study possible differences we show BSS specific frequencies for the two clusters on the same figure (see Figure 6). The radial coordinate has been expressed as a function of the core radius r_c . Using our observed star counts we have found values of $r_c = 21''$ and $r_c = 24''$ for 47 Tuc and M3, respectively. In order to derive the core radius we followed the same procedure shown in Ferraro et al (2003b). All stars brighter than the cluster MS-TO have been used to derive the star density profile that was then fit by the projected star density obtained from a standard isotropic single-mass King-model. The full discussion of the star density profile for both (and a few other) clusters will be presented in a forthcoming paper (Ferraro et al 2003, in preparation). A typical uncertainty of $\pm 2''$ can be assumed in the r_c determination. Note that the value assumed for 47 Tuc is consistent with that ($r_c = 24'' \pm 2''$) recently obtained by Howell, Guhathakurta & Gilliland (2000) in a review discussing the most recent determinations of the core radius of 47 Tuc by using HST. Some points about Figure 6 are worth noting: (1) the central values are similar; (2) while the BSS specific frequency decreases in both clusters as r increases from 0 to $\sim 4r_c$ the decrease is much larger in M3. In 47 Tuc it is a factor of 5.5 dropping from 2.64 down to 0.48; in M3 the drop is a factor of 15 (from 2.76 to 0.2). (3) the main difference in the two distributions is that the specific frequency minimum in 47 Tuc appears to be much broader than that observed in M3. In 47 Tuc the depletion zone extends from $\sim 4r_c$ to 20 – $22r_c$ and with the upturn of the BSS density occurring at $\sim 25r_c$, while in M3 the BSS specific frequency is already rising at $\sim 8r_c$.

5. Discussion

F97 argued that the bimodal distribution of BSS in M3 was evidence that two formation scenarios were at action in the same cluster: the Exterior BSS (EBSS) arising from mass transfer in primordial binaries and the Central BSS (CBSS) arising from stellar interactions which lead to mergers. As had been earlier noted by Bailyn & Pinsonneault (1995), the EBSS and CBSS luminosity functions differed in the sense theoretically expected for two mechanisms.

One difficulty with primordial binaries as a source for the EBSS is that one ordinarily

would expect that they would have settled to the cluster centers since relaxation times are typically less than 1 Gyr (Djorgovski 1993). Simulations to address the question of how many primordial binaries can form in the external regions of the cluster and how long primordial binaries with mass approaching twice the turnoff mass could remain in the outer parts of a cluster are now in progress (M. Mapelli et al 2003, in preparation).

Sigurdsson et al. (1994) offered another explanation for the bimodal BSS distribution in M3. They suggested that the EBSS were formed in the core and then ejected into the outer regions by the recoil from the interactions. Those binaries which get kicked out to a few r_c rapidly drift back to the center of the cluster due to mass segregation, leading to a concentration of BSS near the center and a paucity of BSS in the outer parts of this region. More energetic kicks will take the BSS to larger distances; these stars require much more time to drift back toward the core and may account for the overabundance of BSS at large distance.

How does the discovery of a bimodal radial distribution of BSS in 47 Tuc affect these arguments? Dynamically 47 Tuc is quite different from M3: its central density is 40 times larger (Pryor & Meylan 1993), and its core is rich in X-ray binaries, millisecond pulsars, and other interaction products (Ferraro et al. 2001; Grindlay et al. 2001; Camilo et al. 2000; Edmonds et al 2003). We have already shown (Ferraro et al. 2003a) that CBSS populations cannot be characterized by a simple parameter like collision rate, so the fact that CBSS in 47 Tuc and M3 have comparable specific frequencies should not come as a surprise.

It should be noted that an BSS specific frequency upturn similar to that observed in 47 Tuc and M3 has been detected also in M55 (Zaggia et al. 1997). This is of particular significance because M55 has a low central density—0.1 that of M3. Note that although the data set presented by Zaggia et al. for M55 are ground based observations and covered only a quadrant of the cluster, there is at least preliminary evidence that a upturn is present also in a low density cluster like M55. We note that the effect found by Zaggia et al in M55 could be even stronger since ground-based observations tend to hide BSS in the central region of the cluster. For example ground based observations of the center of M3 led Bolte et al. (1993) to claim depletion of BSS in the center whereas *HST* observations eventually found a peak. M55 is surely less concentrated than M3, but still intermediate crowding conditions and the presence of highly saturated giants in the center can produce some level of incompleteness at the BSS level.

The implications of the bimodality and relatively large populations of EBSS are not yet clear beyond the fact that EBSS may be fairly common and form in diverse clusters. If the BSS bimodality in M55 is confirmed, we will be faced with the result that clusters with central densities ranging over a factor of 400 can produce a bimodal BSS distributions. Any

dynamical model like that of Sigurdsson et al. would seem more applicable to 47 Tuc than M3. It would be a real stretch to reach the dynamical conditions in M55.

Given these factors it seems even more likely that primordial binaries play a fundamental role in the BSS formation mechanism. Better information on the abundance of primordial binaries in clusters and their survival rate at a given distance from the cluster center is essential. In 47 Tuc a recent extensive search for binary stars in the core (Albrow et al 2001) has led to an overall binary frequency of $14\% \pm 4\%$. Their Fig. 21 shows that the binaries appear to be significantly more centrally concentrated with respect to the normal cluster stars but less concentrated than the BSS. Hence, if the cluster is in dynamical equilibrium, the CBSS are among the heaviest visible stellar components in the core of 47 Tuc. Albrow et al. also note that the W UMa stars form a sequence in the CMD which like that which would be expected for equal mass binaries. The brightest lie in the BSS region of the CMD. Since W UMa systems are contact binaries they may well merge to become BSS.

Unfortunately, binary populations have been measured in only a few additional clusters (most notably NGC 6752, NGC 288), and they probably have diverse origins: (*i*) in the core of NGC 6752 (Rubenstein & Bailyn 1997) the binaries are probably not primordial, since NGC 6752 is such a dynamically evolved cluster (Ferraro et al. 2003b, and references there-in); (*ii*) in the low density cluster NGC 288 (Bellazzini et al. 2002), the binaries are probably primordial. Despite the much longer relaxation time of NGC 288, the binaries have all settled to within the inner half light radius; The technique used by Rubenstein & Bailyn (1997) and Bellazzini et al. (2002) requires only modest *HST* observation time and should be applicable to any cluster. Even though such studies of the binary populations are painful, we need more.

Clearly, it is desirable to have full BSS surveys for more clusters. It may well be a fluke that the first two clusters to be fully surveyed have bimodal distributions. We have pointed out (Ferraro et al. 2003a) that all properly studied clusters have CBSS. The existence of EBSS in M3 (Sandage 1953) marked the discovery of BSS. Similarly there is clear evidence for EBSS in ground based CMDs of 47 Tuc (Sills et al. 2000; Grundahl et al. 2002; Kaluzny et al. 1998). Quite possibly all clusters with significant EBSS populations are bimodal. On the other hand, high quality CMDs of other clusters like M5 (Sandquist et al. 1996) and M80 (Brocato et al. 1998) show evidence for few if any EBSS. If more careful studies of such clusters do not reveal a yet undetected EBSS population, we will have to search for a mechanism which produces bimodal radial BSS distributions in some clusters but not in others.

The population of BSS discovered here opens a new window for the investigation of the origin and the formation mechanism of BSS in GGCs. In fact, this discovery suggests that

the *peculiar* radial distribution firstly found in M3 is much more *common* than was thought. Possibly in a few years we will refer to Figure 5 as the typical radial BSS distribution in stellar aggregates. In the meanwhile let us still refer to it as *peculiar* until its generality can be finally addressed.

We are now exploiting the wealth of information in the large dataset presented here by performing an extensive spectroscopic survey of the BSS population in 47 Tuc using the new multi-fiber Spectrograph FLAMES at the ESO-Very Large Telescope. These data should be highly informative. For instance, radial velocity determinations for a significant number of EBSS would help to clarify their origin: if the EBSS were ejected from the cluster center their velocity dispersion should be low because they are expected to be observed near the apocenter of an highly elliptical orbit; if EBSS arise from primordial binaries the velocity dispersion might be close to the Keplerian velocity (circular orbits which avoid the cluster center might allow the binaries to remain in the exterior) and show small variations due to low mass companions. The same spectra could lead to many mass estimates: so far the only BSS with a measured mass ($1.7 \pm 0.4 M_{\odot}$) is in 47 Tuc and was obtained with *HST* (Shara et al. 1997).

We warmly thank Paolo Montegriffo for assistance during the astrometry procedure and Michela Mapelli and Andrea Possenti for useful discussion. The financial support of the Agenzia Spaziale Italiana (ASI) and the Ministero dell’Istruzione, dell’Università e della Ricerca is kindly acknowledged. This research has made use of the GSCII catalog which has been produced by the Space Telescope Science Institute and the Osservatorio Astronomico di Torino and of the ESO/ST-ECF Science Archive facility which is a joint collaboration of the European Southern Observatory and the Space Telescope - European Coordinating Facility. RTR is partially supported by STScI grant GO-8709 and NASA LTSA grant NAG 5-6403.

REFERENCES

- Albrow, M.D., Gilliland, R.L., Brown, T.M., Edmonds, P.D., Guhathakurta, P., Sarajedini, A., 2001, ApJ, 559, 1060
- Bailyn, C.D. 1995, ARA&A, 33, 133
- Bailyn, C. D. & Pinsonneault, M. H. 1995, ApJ, 439, 705
- Bellazzini, M., Fusi Pecci, F., Messineo, M., Monaco, L., & Rood, R. T. 2002, AJ, 123, 1509

- Bolte, M., Hesser, J.E., & Stetson, P.B., 1993, ApJ, 408, L89
- Brocato, E., Castellani, V., Scotti, G. A., Saviane, I., Piotto, G., & Ferraro, F. R. 1998, A&A, 335, 929
- Buonanno, R., Buscema, G., Corsi, C.E., Ferraro, I., & Iannicola, G., 1983, A&A, 126, 278
- Camilo, F., Lorimer, D. R., Freire, P., Lyne, A. G., & Manchester, R. N. 2000, ApJ, 535, 975
- de Marchi, G., Paresce, F., & Ferraro, F. R. 1993, ApJS, 85, 293
- Djorgovski, S. 1993, ASP Conf. Ser. 50: Structure and Dynamics of Globular Clusters, 373
- Djorgovski, S. & Meylan, G. 1993, ASP Conf. Ser. 50: Structure and Dynamics of Globular Clusters, 325
- Edmonds, P.D., Gilliland, R.L., Heinke, C.O., Grindlay, J.E., 2003, ApJ, in press, astro-ph/0307187
- Ferraro, F.R., Paltrinieri, B., Fusi Pecci, F., Cacciari, C., Dorman, B., Rood, R.T., Buonanno, R., Corsi, C.E., Burgarella, D., Laget, M., 1997, A&A, 324, 915
- Ferraro, F.R., Paltrinieri, B., Rood, R.T., Dorman, B., 1999, ApJ, 522, 983
- Ferraro, F. R., Pecci, F. F., Cacciari, C., Corsi, C., Buonanno, R., Fahlman, G. G., & Richer, H. B. 1993, AJ, 106, 2324
- Ferraro, F. R., D'Amico, N., Possenti, A., Mignani, R. P., & Paltrinieri, B. 2001, ApJ, 561, 337
- Ferraro, F. R., Sills, A., Rood, R. T., Paltrinieri, B., & Buonanno, R. 2003a, ApJ, 588, 464
- Ferraro, F. R., Possenti, A., Sabbi, E., Lagani, P., Rood, R. T., D'Amico, N., & Origlia, L. 2003b, ApJ, in press
- Grindlay, J. E., Heinke, C., Edmunds, P. D., & Murray, S. S. 2001, Science, 292, 2290
- Grundahl, F., Stetson, P. B., & Andersen, M. I. 2002, A&A, 395, 481
- Guhathakurta, P., Yanny, B., Schneider, D.P., Bahcall, J.N., 1992, ApJ 104, 1790
- Holtzmann, J.A., Burrows, C.J., Casertano, S., Hester, J.J., Trauger, J.T., Watson, A.M., & Worthey, G. 1995, PASP, 107, 1065.

- Howell, J.H., Guhathakurta, P., Gilliland, R.L., 2000., PASP, 112, 1200
- Kaluzny, J., Wysocka, A., Stanek, K. Z., & Krzeminski, W. 1998, Acta Astronomica, 48, 439
- Knigge, C., Zurek, D. R., Shara, M. M., & Long, K. S. 2002, ApJ, 579, 752
- Lemon, D.J., Wyse, R.,F.G., Liske, J., Driver, S.P., Horne, K., 2003, MNRAS, in press, astro-ph/0308200
- Momany, Y., et al., 2001, A&A, 379, 436
- Montegriffo, P., Ferraro, F. R., Fusi Pecci, F. & Origlia. L. 1995, MNRAS, 276, 739
- Pryor, C. & Meylan, G. 1993, ASP Conf. Ser. 50: Structure and Dynamics of Globular Clusters, 357
- Ratnatunga, K.U., Bahcall, J.N., 1985, ApJSS, 59, 63
- Renzini, A., Buzzoni, A. 1986 in *Spectral Evolution of Galaxies*, C. Chiosi& A. Renzini (eds), Dordrecht: Reidel, p.135.
- Rubenstein, E. P., & Bailyn, C. D., 1997, ApJ, 474, 701
- Sandage, A. R. 1953, AJ, 58, 61
- Sandquist, E. L., Bolte, M., Stetson, P. B., & Hesser, J. E. 1996, ApJ, 470, 910
- Schechter, P. L.,Mateo, M., & Saha, A. 1993, PASP, 105, 1342
- Shara, M. M., Saffer, R. A., & Livio, M. 1997, ApJ, 489, L59
- Sigurdsson, S., Davies, M. B., & Bolte, M. 1994, ApJ, 431, L115
- Sills, A., Bailyn, C. D., Edmonds, P. D., & Gilliland, R. L. 2000, ApJ, 535, 298
- Trager, S. C., Djorgovski, S., & King, I. R. 1993, ASP Conf. Ser. 50: Structure and Dynamics of Globular Clusters, 347
- Unavane, M., Wyse, R.F.G., Gilmore, G., MNRAS, 278, 727
- Zaggia, S., Piotto, G., Capaccioli, M., 1997, A&A, 327, 1004
- Zoccali, M., et al., 2001, ApJ, 553, 733

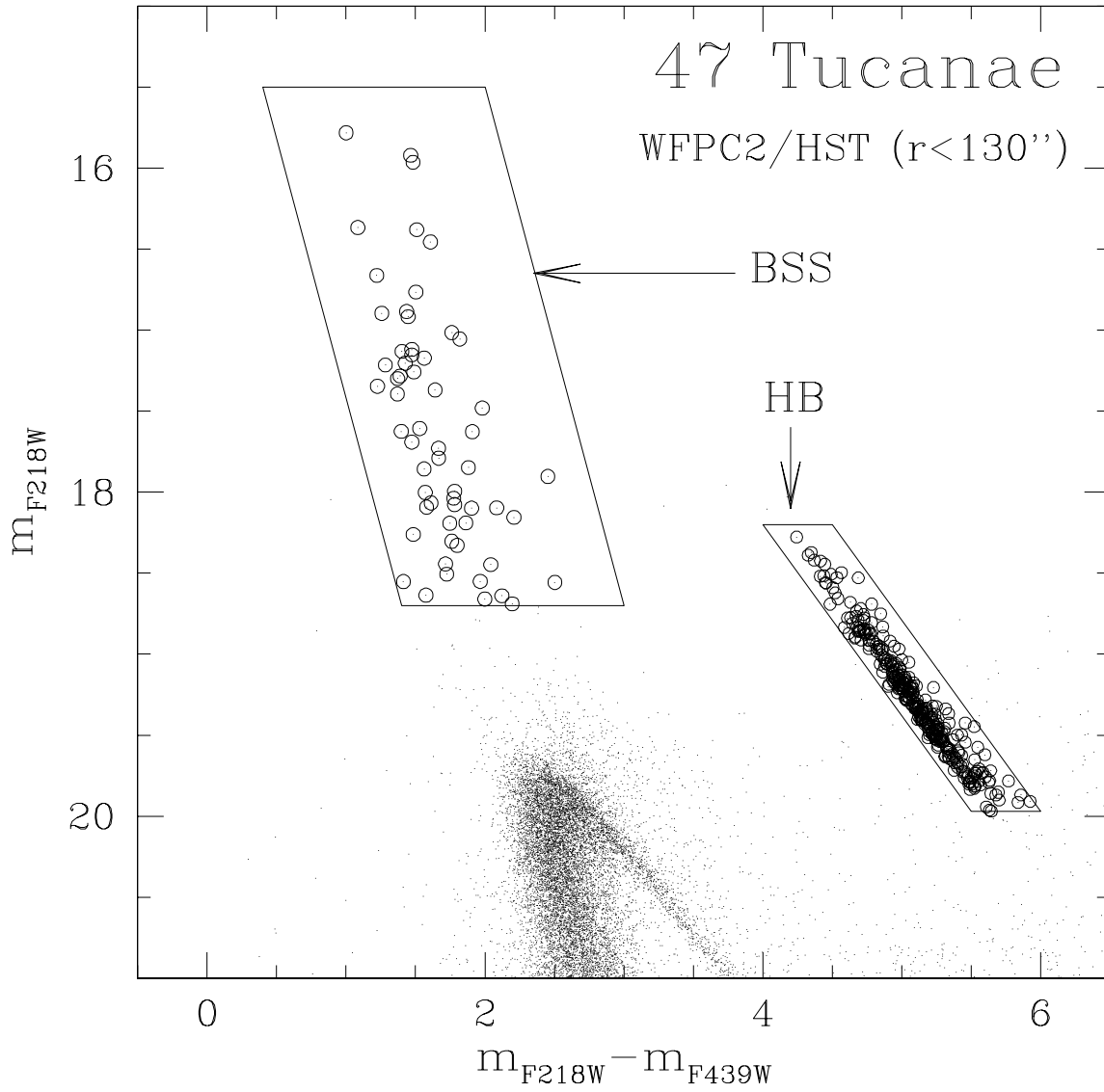


Fig. 1.— $(m_{218}, m_{218} - m_{439})$ CMD for the central region of 47 Tuc ($r < 130''$) from WFPC2/HST observations. The two selection boxes for the BSS and the reference (HB) population are shown.

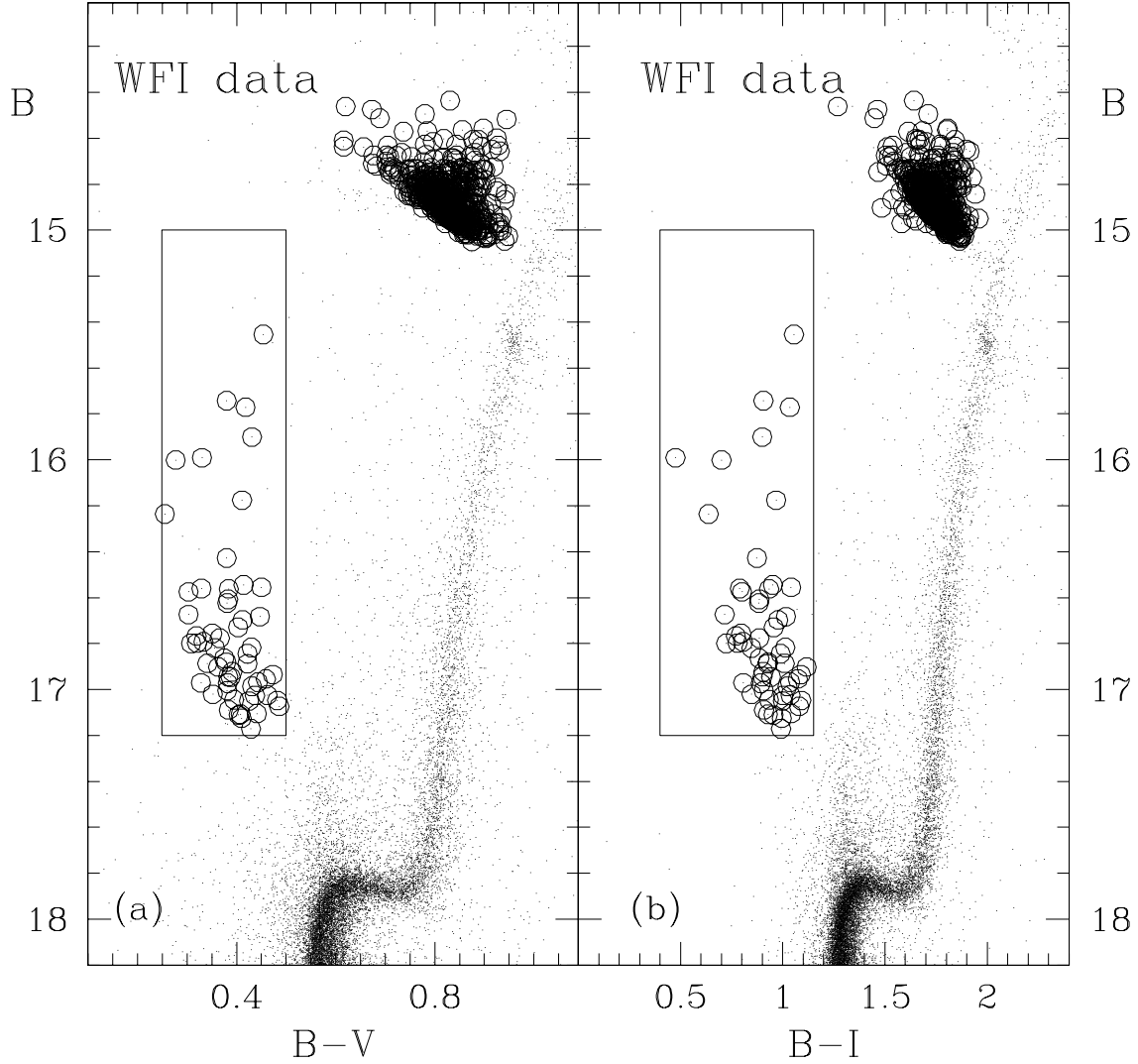


Fig. 2.— $B, B - V$ (Panel (a)) and $B, B - I$ (Panel (b)) CMDs for the external part of 47 Tuc ($130'' < r < 1500''$) from ground-based (WFI) observations. As in Figure 1 stars selected in the BSS and in the reference (HB) population are marked with empty circles.

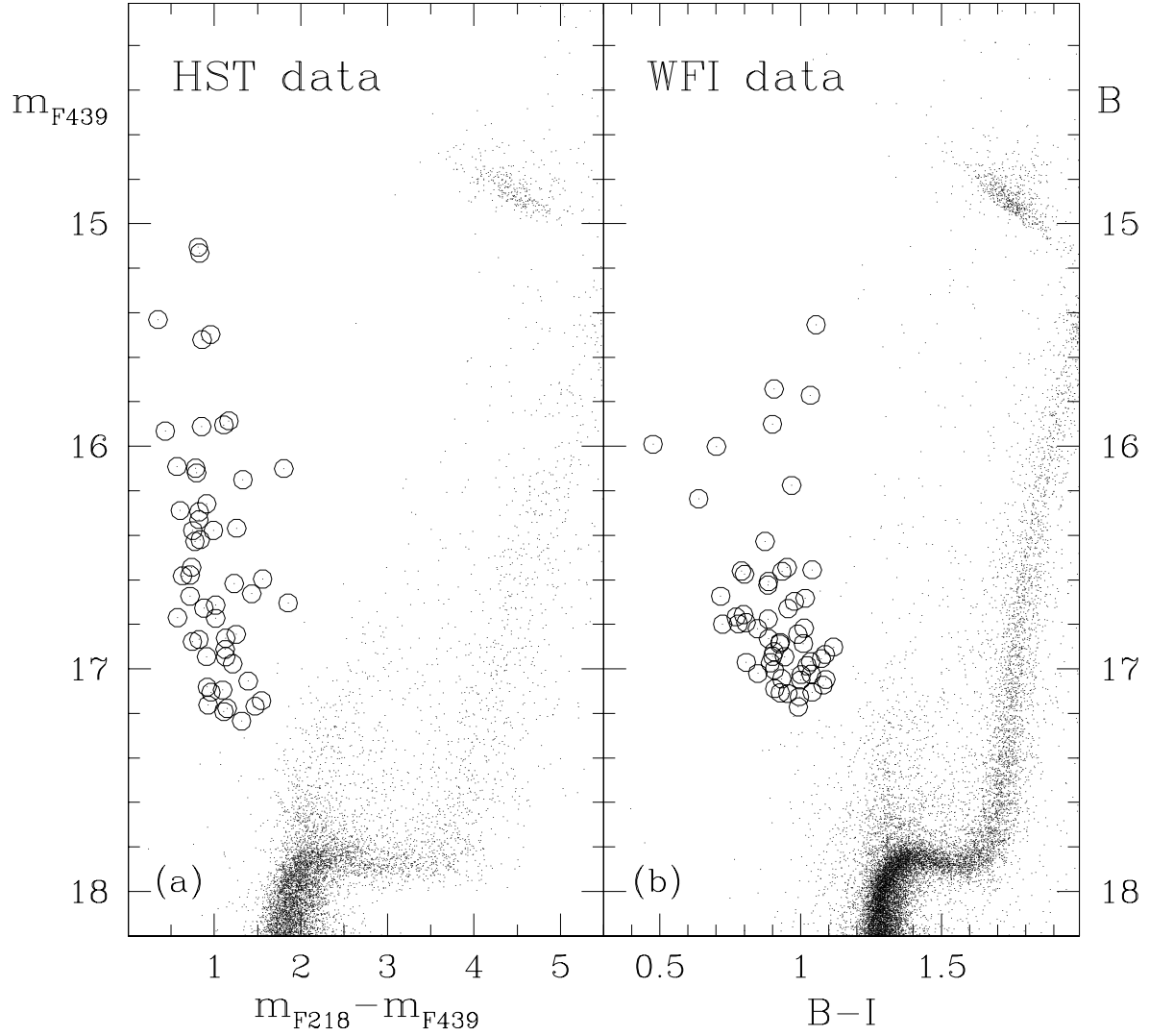


Fig. 3.— Direct comparison between the HST (*Panel (a)*) and the ground-based WFI sample (*Panel (b)*). As in Figure 1 and 2 stars selected in the BSS population are marked with empty circles. As can be seen the selected BSS samples are fully homogeneous.

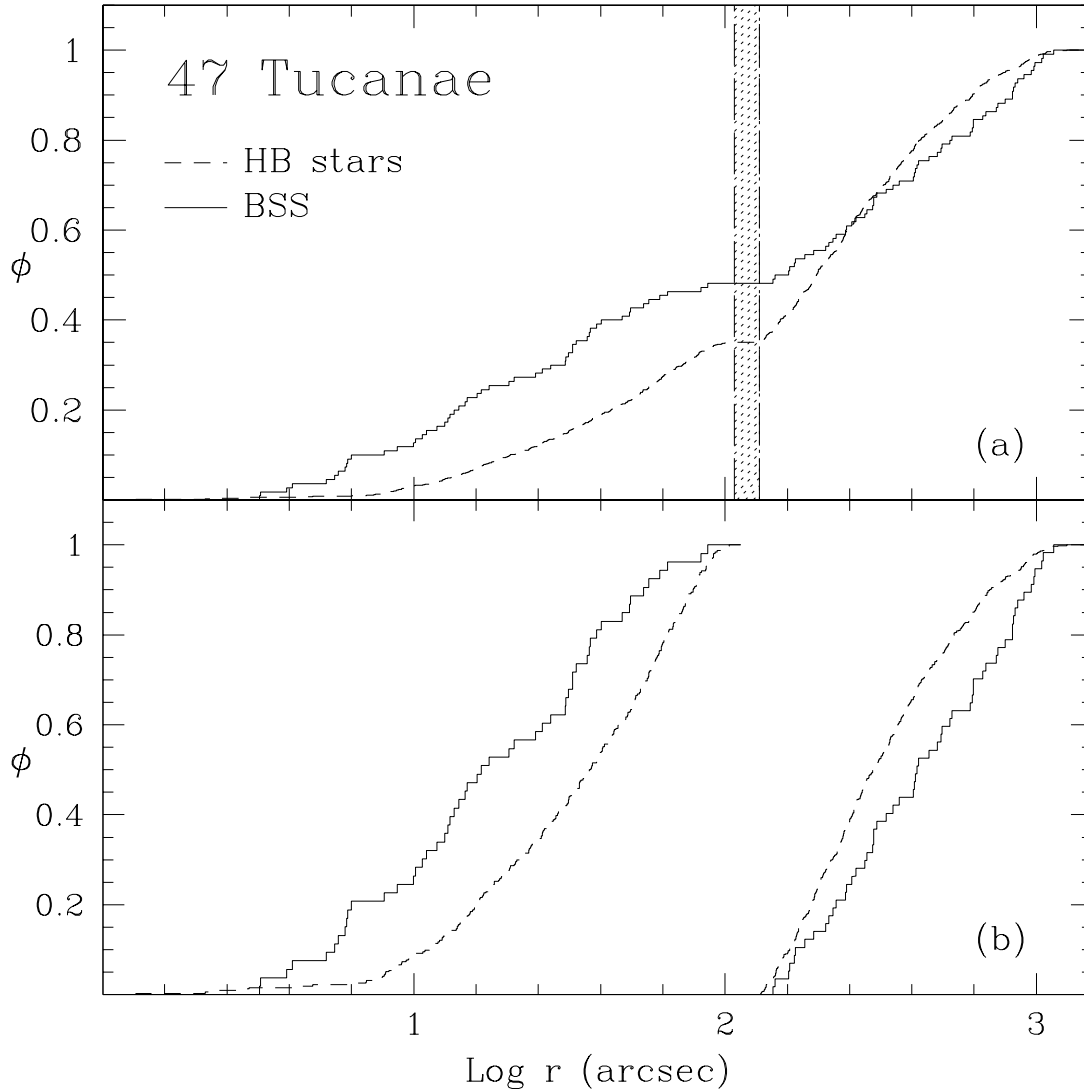


Fig. 4.— *Panel (a)*: Cumulative radial distributions for the *bright* BSS (solid line) with respect to the HB stars (dashed line) as a function of their projected distance (r) from the cluster center for the global sample. The vertical dotted line distinguish the cluster regions observed with HST from the regions observed from the ground. *Panel (b)*: The same as *panel (a)* for two radial subsamples.

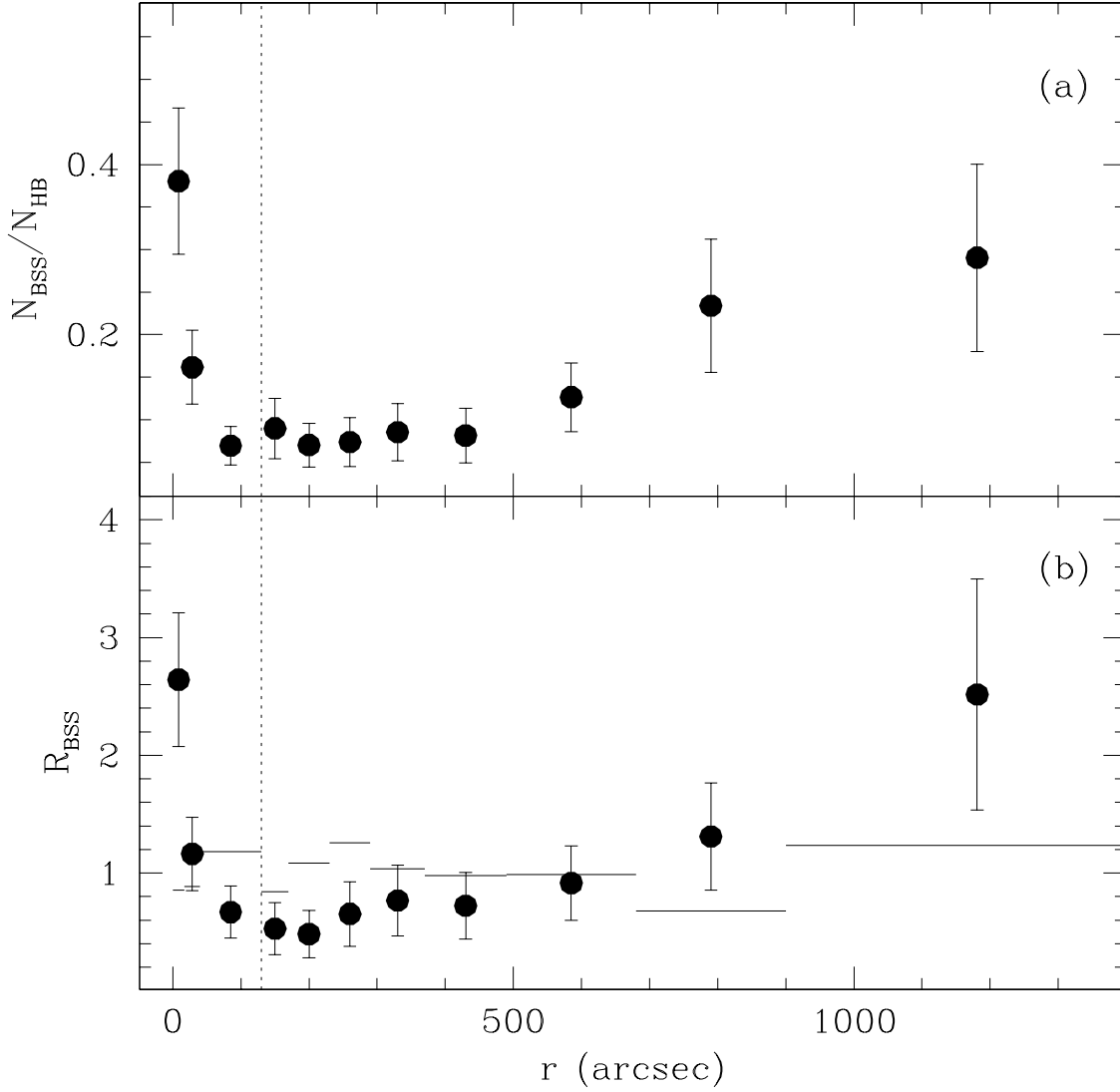


Fig. 5.— *Panel (a)*: The relative frequency of BSS with respect to HB stars is plotted as a function of the distance from the cluster center for each of the 11 concentric annuli defined in the text. *Panel (b)*: The specific frequency of BSS (see text) is plotted. The horizontal lines show the specific frequency for the HB reference population. The vertical dotted line distinguish the cluster regions observed with HST from the regions observed from the ground.

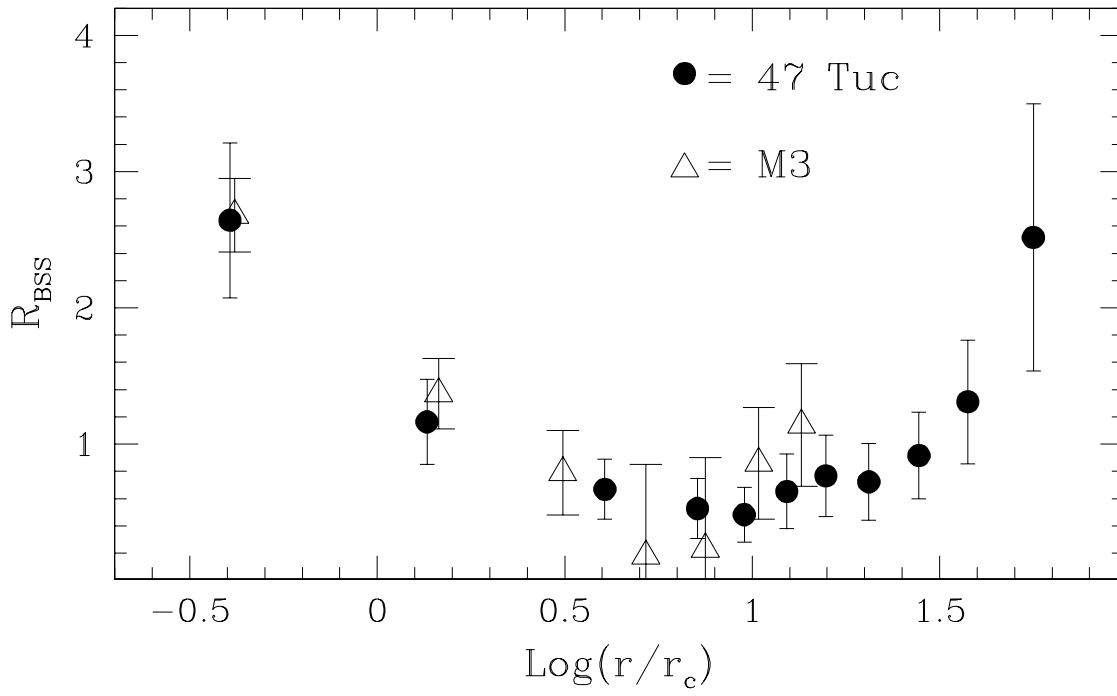


Fig. 6.— The specific frequency of BSS in 47 Tuc (filled circles) is compared with that found in M3 (empty triangles). The radial coordinate is expressed in unit of core radii r_c .

Table 1. Numbers and relative frequencies for BSS and HB stars.

r	N_{BSS}	N_{HB}	$N_{\text{BSS}}/N_{\text{HB}}$	$L_{\text{annulus}}/L_{\text{TOT}}$	R_{BSS}	ϵ_{BSS}	R_{HB}	ϵ_{HB}
0"-17"	27	71	0.38	0.09	2.64	0.57	0.85	0.11
17"-40"	16	99	0.16	0.12	1.16	0.31	0.88	0.09
40"-130"	10	144	0.07	0.14	0.67	0.22	1.18	0.11
130"-170"	6	78	0.09	0.10	0.53	0.22	0.84	0.10
170"-230"	6	110	0.07	0.11	0.48	0.20	1.09	0.11
230"-290"	6	94	0.07	0.08	0.65	0.27	1.26	0.14
290"-370"	7	77	0.09	0.08	0.77	0.30	1.04	0.12
370"-490"	7	77	0.08	0.09	0.72	0.28	0.98	0.12
490"-680"	9	79	0.13	0.09	0.92	0.32	0.99	0.12
680"-900"	9	38	0.23	0.06	1.31	0.45	0.68	0.11
900"-1462"	7	28	0.29	0.03	2.52	0.98	1.24	0.24